文章编号：1001-9014(XXXX)XX-0001-06

DOI:10.11972/j.issn.1001-9014.XXXX.XX.001

# Broadband high-extinction-ratio nonvolatile optical switch based on phase change material

LIANG Kai[1,2], YUE Wen-Cheng[1*], XU Fan[3], ZHU Qian-Nan[1,2], ZHANG Jian-Min[1,2], WANG Shu-Xiao[1], CAI Yan[1]

(1. State Key Laboratory of Materials for Integrated Circuits, Shanghai Institute of Microsystem and Information Technology, Chinese Academy of Sciences, Shanghai 200050, China;
2. University of the Chinese Academy of Sciences, Beijing 100049, China;
3. School of Microelectronics, Shanghai University, Shanghai 201800, China)

**Abstract**: In this paper, we present a broadband, high-extinction-ratio, nonvolatile 2×2 Mach-Zehnder interferometer (MZI) optical switch based on the phase change material $Sb_2Se_3$. The insertion loss (IL) is 0.84 dB and the extinction ratio (ER) reaches 28.8 dB at the wavelength of 1550 nm. The 3 dB bandwidth is greater than 150 nm. Within the 3 dB bandwidth, the ER is greater than 20.3 dB and 16.3 dB at bar and cross states, respectively. The power consumption for crystallization and amorphization of $Sb_2Se_3$ is 105.86 nJ and 49 nJ, respectively. The switch holds significant promise for optical interconnects and optical computing applications.

**Key words**: photonic integration, optical switch, phase change materials

# 基于相变材料的宽带高消光比非易失性光开关

梁 凯[1,2], 岳文成[1*], 许 凡[3], 朱倩男[1,2], 张建民[1,2], 王书晓[1], 蔡 艳[1]

(1. 中国科学院上海微系统与信息技术研究所集成电路材料全国重点实验室,上海 200050;
2. 中国科学院大学,北京 100049;
3. 上海大学微电子学院,上海 201800)

**摘要**:本文介绍了一种基于相变材料 $Sb_2Se_3$ 的宽带、高消光比、非易失的 2×2 马赫-增德尔干涉仪(MZI)型光开关。在波长为 1550 nm 时,插入损耗(IL)为 0.84 dB,消光比(ER)达到 28.8 dB。器件的 3 dB 带宽大于 150 nm。在 3 dB 带宽内,直通态和交叉态的消光比分别大于 20.3 dB 和 16.3 dB。$Sb_2Se_3$ 的晶化和非晶化功耗分别为 105.86 nJ 和 49 nJ。该宽带高消光比非易失性光开关在光互连和光计算中有极大的应用潜力。

**关 键 词**:光子集成;光开关;相变材料

**中图分类号**:O439　　**文献标识码**:A

## Introduction

With the rapid development of artificial intelligence, data traffic is experiencing exponential growth[1,2]. The demand for parallelism and data bandwidth is increasing, and reducing power consumption and economic costs is becoming more critical. Optical data transmission offers advantages over traditional electrical signals in high-speed, high-bandwidth applications[3]. Optical switches are one of the fundamental components in integrated photonic circuits, functioning to perform physical switching and logical operations on optical signals in transmission lines or integrated photonic circuits. The Mach-Zehnder interferometer (MZI) is a common structure in optical switches. It offers advantages such as wide operational bandwidth, low loss, high fabrication tolerance, and insensitivity to temperature[4]. Traditional MZI silicon-based optical switches typically

**Received date**: 2025-01-02, **revised date**: 2025-02-12　　**收稿日期**:2025-01-02,**修回日期**:2025-02-12

**Foundation items**: Supported by the National Natural Science Foundation of China (62204250) and the Autonomous deployment project of State Key Laboratory of Materials for Integrated Circuits (SKLJC-Z2024-A05).

**Biography**: Liang Kai (1999-), male, Shanghai, Master. Research area involves the design of silicon-based optoelectronic devices.

* **Corresponding authors**: E-mail: wencheng.yue@mail.sim.ac.cn; yan.cai@mail.sim.ac.cn

achieve switching functionality by altering the effective refractive index of optical modes through the thermo-optic effect or plasma dispersion effect. However, optical modulation based on the plasma dispersion effect or thermo-optical effect is weak (usually $\Delta n < 0.01$)[5], which results in large footprint or high power consumption. Moreover, silicon-based thermo-optical and electro-optical switches require continuous energy to maintain ON/OFF state, which makes high static power consumption.

Phase change materials (PCMs) have attracted a lot of attention due to its excellent properties, such as high refractive index contrast between crystalline and amorphous states, nonvolatility, reversibility and high repeatability[6-10]. $Ge_2Sb_2Te_5$ (GST) is one of the most commonly used PCMs in silicon-based optical switches due to its significant refractive index contrast ($\Delta n \approx 2.8$ at 1550 nm) between crystalline and amorphous states[11-15]. However, the imaginary part of the refractive index of GST is large, which is 1.08 and 0.12 at crystalline and amorphous states at 1550 nm[9], respectively. This will introduce high loss in the MZI optical switch and limit its applications. Amorphous (Am-) and crystalline (Cr-) $Sb_2Se_3$ both have low extinction coefficients and exhibit large optical contrast ($\Delta n \approx 0.77$ at 1550 nm) in the near infrared wavelength range, making it highly promising for applications in optical switches[16]. In this work, we proposed a broadband high-extinction-ratio 2×2 MZI nonvolatile optical switch based on $Sb_2Se_3$. The introduction of a π/2 pre-biased waveguide structure reduces the required length of $Sb_2Se_3$ to change the ON/OFF state of the switch, which reduces the absorption loss of crystalline $Sb_2Se_3$ and lowers the power consumption for phase transition of $Sb_2Se_3$. The loss is 0.84 dB at the wavelength of 1550 nm for both bar and cross states. The power consumption is 105.86 nJ and 49 nJ for crystallization and amorphization of $Sb_2Se_3$, respectively. The symmetric integration of $Sb_2Se_3$ in both phase-shift arms improves the extinction ratio (ER). The ER reaches 28.8 dB at the wavelength of 1550 nm. The proposed 2×2 MZI nonvolatile optical switch also has a wide bandwidth of greater than 150 nm.

## 1 Design of device

The designed 2×2 MZI nonvolatile optical switch based on low-loss $Sb_2Se_3$ consists of two 2×2 multimode interferometers (MMIs) and phase-shift arms, as shown in Fig. 1(a). To reduce the crosstalk at the MMI output, curved waveguides with radius of 10 μm were used to connect MMIs and phase-shift arms. MMI has the advantages of wide bandwidth and large fabrication tolerance. Two 2×2 MMIs are used as power splitter and combiner, respectively. The phase shifters are composed of Si-$Sb_2Se_3$ hybrid waveguides (Fig. 1(b)). When only one phase-shift arm integrates phase-change material, the large loss difference between the upper and lower phase-shift arms will reduce ER, especially in Cr-$Sb_2Se_3$. Thus, to improve ER, $Sb_2Se_3$ is integrated in both the upper and lower phase-shift arms. To shorten the length of $Sb_2Se_3$, which can reduce the absorption loss especially of crystalline $Sb_2Se_3$ and lower the power consumption for phase transition of $Sb_2Se_3$, we introduced a π/2 pre-biased waveguide structure in the lower phase-shift arm[17]. In this way, only a π/2 phase shift needs to be achieved by the phase transition of $Sb_2Se_3$ to control the ON/OFF state of the switch. Through the π/2 pre-biased structure has been reported in reference [17], it works at the wavelength of 2 μm. We designed and optimized the π/2 pre-biased structure at the wavelength of 1550 nm, and firstly introduced it in the $Sb_2Se_3$ optical switch. The π/2 pre-biased structure contains two symmetric tapered waveguide whose width transits from $w$ = 500 nm to $w_2$ = 544 nm with a total length $L$ of 12 μm (Fig. 1(c)). Then, the Si-$Sb_2Se_3$ hybrid waveguide was optimized by the finite element method (FEM). Considering compatibility with the complementary metal-oxide-semiconductor (CMOS) fabrication process and single-mode condition, we determined the silicon waveguide dimensions to be 220 nm in thickness and 500 nm in width. At the wavelength of 1550 nm, the refractive index of Si and $SiO_2$ is 3.476 + $i$0, 1.444 + $i$0, respectively[18, 19]. We fabricated layered $Sb_2Se_3$ and measured its optical constants at amorphous and crystalline states by

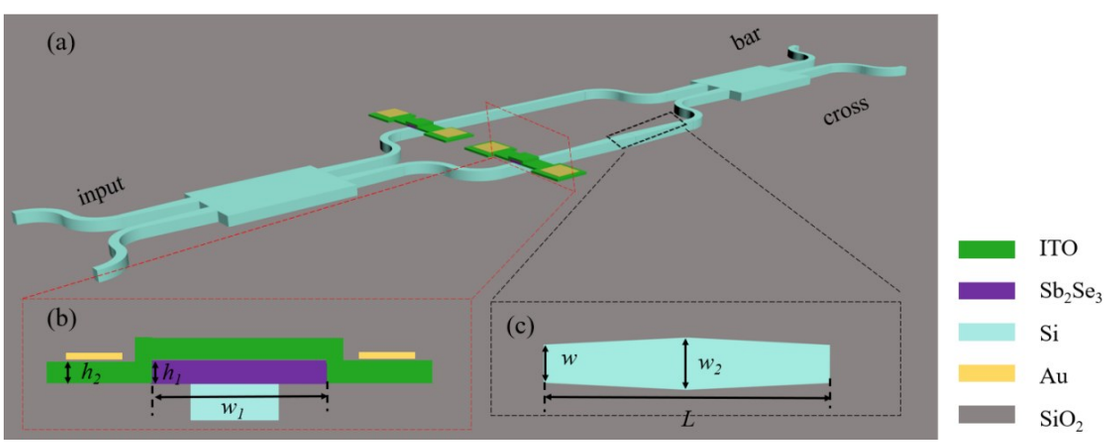


Fig. 1. (a) Schematic diagram of the proposed 2×2 MZI nonvolatile optical switch. (b) Cross-section of the Si-$Sb_2Se_3$ hybrid waveguide with the ITO heater. (c) Schematic diagram of the π/2 pre-biased waveguide structure

图 1. (a) 2×2 MZI 型非易失性光开关结构示意图。(b) 带有 ITO 加热器的 Si-$Sb_2Se_3$ 混合波导截面图。(c) π/2 预偏置波导结构示意图

ellipsometer, as shown in Fig. 2. The measurement results indicate that the refractive index of amorphous and crystalline $Sb_2Se_3$ is 3.321 + *i*0 and 4.024 + *i*0.0087 at the wavelength of 1550 nm, respectively. The change of effective refractive index difference ($\Delta n_{eff}$) of transverse electric (TE) mode in the Si-$Sb_2Se_3$ hybrid waveguide at the amorphous and crystalline states with the size of $Sb_2Se_3$ is shown in Fig. 3(a). Clearly, $\Delta n_{eff}$ increases along with the thickness $h_1$ of $Sb_2Se_3$, while firstly increases with the width $w_1$ of $Sb_2Se_3$ and then tends to be stable when $w_1 > 1$ μm. According to the phase calculation formula:

$$\Delta\varphi = \frac{2\pi\Delta n_{eff}}{\lambda} \times L, \tag{1}$$

the larger $\Delta n_{eff}$, the shorter the required length of $Sb_2Se_3$ to achieve the desired phase shift. So, we determined the width $w_1$ of $Sb_2Se_3$ to be 1 μm. At the wavelength of 1550 nm, the required length $L_{(\pi/2)}$ of $Sb_2Se_3$ to achieve π/2 phase shift at different size of $Sb_2Se_3$ is shown in Fig. 3(b). $L_{(\pi/2)}$ reduces as the thickness $h_1$ of $Sb_2Se_3$ increases. The absorption loss of the Si-$Sb_2Se_3$ hybrid waveguide can be calculated by $\alpha_{dB}L_{(\pi/2)}$, where $\alpha_{dB}$ is the power propagation loss in dB/μm. $\alpha_{dB}$ can be converted from the propagation loss constant $\alpha$ ($\mu m^{-1}$) by the formula $\alpha_{dB} = 20\alpha / \ln 10$ (dB/μm)[20]. According to $\alpha = 2\pi k_{neff}/\lambda$, so $\alpha_{dB}$ can be calculated by $\alpha_{dB} = 40\pi k_{neff}/(\lambda \ln 10)$ (dB/μm), where $k_{neff}$ is the imaginary part of effective refractive index of the Si-$Sb_2Se_3$ hybrid waveguide at the crystalline state and is shown in Fig. 3(c). So, we can derive the absorption loss of the Si-$Sb_2Se_3$ hybrid waveguide at different thickness $h_1$ and width $w_1$ of $Sb_2Se_3$, as shown in Fig. 3(d). The absorption loss increases slightly along with the thickness $h_1$ of $Sb_2Se_3$. However, $\Delta n_{eff}$ increases along with $h_1$, as mentioned above. Considering the thicker the PCM, the more difficult the phase transition and the greater the power consumption, the thickness $h_1$ of $Sb_2Se_3$ is chosen to be 50 nm.

The phase transition of $Sb_2Se_3$ is actuated by indium tin oxide (ITO) heater. ITO is compatible with CMOS process and its fabrication process is simple, making it more suitable for applications with large-scale integration

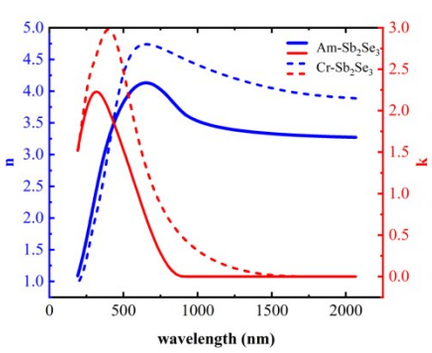


Fig. 2　Optical constants of layered $Sb_2Se_3$ at crystalline and amorphous states measured using ellipsometry in the experiment.
图 2　椭偏仪测量的 Sb2Se3 薄膜在晶态和非晶态下的光学常数

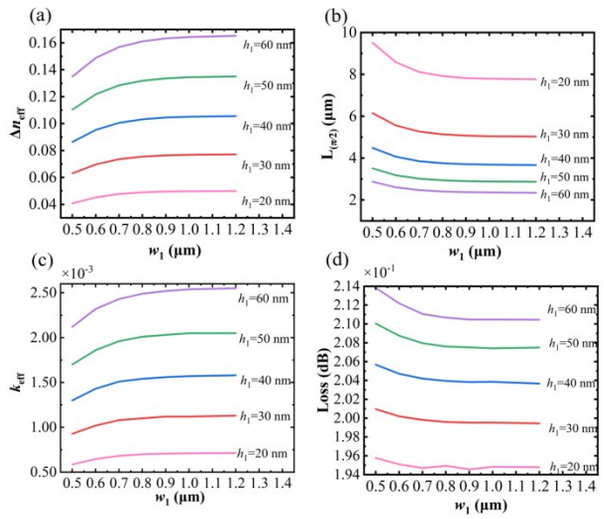


Fig. 3　Structural parameter optimization. (a) Effect of the size of $Sb_2Se_3$ on the difference of effective refractive index ($\Delta n_{eff}$) of the Si-$Sb_2Se_3$ hybrid waveguide at the amorphous and crystalline states. (b) The required length of $Sb_2Se_3$ to achieve π/2 phase shift at different thickness and width of $Sb_2Se_3$. Effect of the size of $Sb_2Se_3$ on the (c) imaginary part ($k_{eff}$) of effective refractive index and (d) absorption loss of the Si-$Sb_2Se_3$ hybrid waveguide at the crystalline state. The optimization was implemented for TE mode at the wavelength of 1550 nm
图 3　结构参数优化。(a) Sb2Se3 处于非晶态和晶态时 Si-Sb2Se3 混合波导有效折射率差 (Δneff) 与 Sb2Se3 的厚度和宽度的变化关系。(b) 实现 π/2 相移所需的 Sb2Se3 长度与 Sb2Se3 的厚度和宽度的变化关系。Sb2Se3 处于晶态时, Si- Sb2Se3 混合波导的 (c) 有效折射率虚部 (keff) 和 (d) 吸收损耗随 Sb2Se3 厚度和宽度的变化关系。以上结果是在 1550 nm 波长下基于 TE 模式得到的

of optical switches[21, 22]. The cross-section of the Si-$Sb_2Se_3$ hybrid waveguide with ITO heater (Si-$Sb_2Se_3$-ITO waveguide) is shown in Fig. 1(b). The introduction of the ITO heater will affect the optical mode, which will further change the required length of $Sb_2Se_3$ to achieve π/2 phase shift and absorption loss at the crystalline state. We optimized the thickness $h_2$ of ITO by FEM. We fabricated the ITO film and measured its optical constant by ellipsometer, as shown in Fig. 4(a). The complex refractive index of ITO is 2.021 + *i* 0.0049 at the wavelength of 1550 nm. Similar to the optimization of the Si-$Sb_2Se_3$ hybrid waveguide, we can derive the required length of the Si-$Sb_2Se_3$-ITO waveguide ($L'_{(\pi/2)}$) and the absorption loss of the Si-$Sb_2Se_3$-ITO waveguide in Cr-$Sb_2Se_3$ according to the simulated effective complex refractive index and corresponding formulas, as shown in Fig. 4(b). The required length reduces as $h_2$ increases, while the absorption loss increases. The shorter the Si-$Sb_2Se_3$-ITO waveguide ($L'_{(\pi/2)}$), the lower the power consumption for the phase transition of $Sb_2Se_3$ and the more beneficial to the miniaturization of the device. To balance the required length and absorption loss, the ITO thickness is chosen to be 30 nm. So only 2.71 μm long $Sb_2Se_3$ at the wavelength of 1550 nm is needed to realize π/2 phase shift (Fig. 4(b)). The simulated cross-section normalized mode profiles of TE mode in the Si-$Sb_2Se_3$-ITO wave-

guide in Cr-$Sb_2Se_3$ and Am-$Sb_2Se_3$ are shown in Fig. 4(c) and Fig. 4(d), respectively.

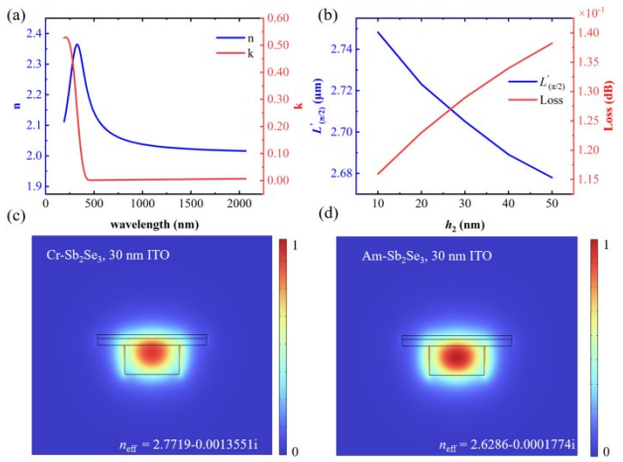


Fig. 4 (a) Optical constant of the fabricated ITO film measured by ellipsometry in the experiment. (b) Effect of ITO thickness on the required length of the Si-$Sb_2Se_3$-ITO waveguide to achieve $\pi/2$ phase shift and the absorption loss of the Si-$Sb_2Se_3$-ITO waveguide at the crystalline state of $Sb_2Se_3$. The cross-section normalized mode profiles of TE mode in the Si-$Sb_2Se_3$-ITO waveguide in (c) Cr-$Sb_2Se_3$ and (d) Am-$Sb_2Se_3$ when $h_1$ = 50 nm, $h_2$ = 30 nm and $w_1$ = 1 μm. The simulation was implemented for TE mode at the wavelength of 1550 nm

图 4 (a) 使用椭偏仪测量的 ITO 薄膜的光学常数。(b) 实现 $\pi/2$ 相移对应的 Si-Sb2Se3-ITO 混合波导长度和 Sb2Se3 处于晶态时 Si-Sb2Se3-ITO 的吸收损耗随 ITO 厚度的变化关系。当 h1 = 50 nm、h2 = 30 nm 和 w1 = 1 μm 时，Si-Sb2Se3-ITO 波导中 (c) Sb2Se3 处于晶态和 (d) Sb2Se3 处于非晶态时 TE 模式的归一化模场分布图。以上结果是在 1550 nm 波长下基于 TE 模式得到的

## 2 Results and discussions

### 2.1 Optical Performance

We used the finite-difference time-domain (FDTD) method to study the optical performance of the proposed 2×2 MZI nonvolatile silicon-based optical switch. When $Sb_2Se_3$ in the lower and upper phase-shift arms are at the crystalline and amorphous states, respectively, the light outputs from the bar port, as shown in Fig. 5(a). The total IL is 0.84 dB and the ER reaches 28.8 dB at the wavelength of 1550 nm (Fig. 5(b)). Inversely, when $Sb_2Se_3$ in the lower and upper phase-shift arms are at the amorphous and crystalline states, respectively, the light outputs from the cross port (Fig. 5(c)) with an IL of 0.84 dB and an ER of 19.8 dB at the wavelength of 1550 nm (Fig. 5(d)). The IL is mainly caused by two reasons. One is the absorption of crystalline $Sb_2Se_3$ and ITO, and the other is the mode mismatch between the Si waveguide and the Si-$Sb_2Se_3$-ITO waveguide. The IL can be further reduced by introducing a coupler structure between the Si waveguide and the Si-$Sb_2Se_3$-ITO waveguide or by designing micro-nano structured $Sb_2Se_3$. As shown in Fig. 5(b), the 3 dB bandwidth of the optical switch is greater than 150 nm at bar state and the ER is greater than 20.3 dB in the 3 dB bandwidth. At cross state, the 3 dB bandwidth is also greater than 150 nm and the ER is greater than 16.3 dB in the 3 dB bandwidth (Fig. 5(d)).

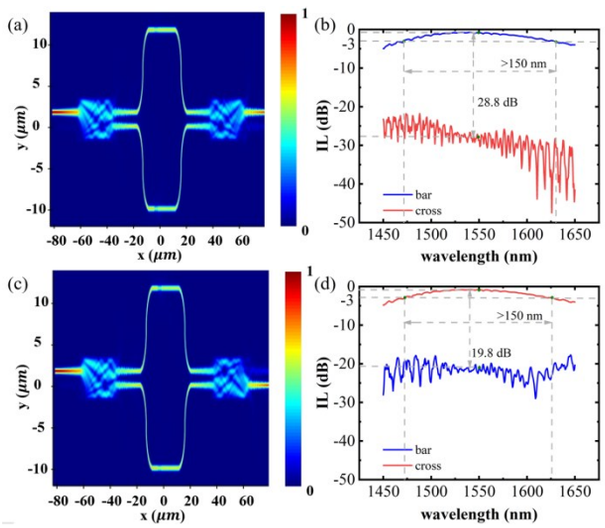


Fig. 5 The simulated electric field distribution diagram of the optical switch at (a) bar state and (c) cross state and the transmission at (b) bar state and (d) cross state

图 5 光开关在 (a) 直通态和 (c) 交叉态时的电场分布图，以及在 (b) 直通态和 (d) 交叉态下的透射谱

### 2.2 Thermal Simulations

We implemented thermal simulation for the phase transition of $Sb_2Se_3$. The resistivity of ITO is $1.6 \times 10^{-3}$ Ω·cm[24]. The material properties used in the thermal simulation are summarized in Table 1. The metal electrode is Au, as shown in Fig. 1(b). The distance from Au to the middle of the Si-$Sb_2Se_3$-ITO waveguide is 2.1 μm to prevent metal absorption. For amorphization, $Sb_2Se_3$ must be rapidly heated to its melting point 893 K and then followed by quick cooling. Therefore, a high and short pulse with 9 V amplitude and 500 ns width is used, as shown by the red line in Fig. 6(a). As the blue line in Fig. 6(a) and Fig. 6(c) show, the temperature of the whole $Sb_2Se_3$ exceeds 893 K, suggesting $Sb_2Se_3$ realizes amorphization completely. The corresponding power consumption is about 49 nJ. For crystallization, the temperature of $Sb_2Se_3$ needs to be controlled between the crystal

**Table 1 Physical parameters of materials used in the thermal simulation.**
**表 1 在热仿真中所用材料的物理参数**

| Materials | $SiO_2$ | Si | Am-$Sb_2Se_3$ | Cr-$Sb_2Se_3$ | ITO |
|---|---|---|---|---|---|
| Density [kg/m$^3$] | 2203 | 2329 | ~6000 | 6500 | 7100[23] |
| Thermal conductivity [W/m·K] | 1.38 | 130 | 0.2 | 0.24 | ~1340[23] |
| Heat capacity at constant pression [J/kg·K] | 746 | 700 | 150 | 150 | 11[23] |

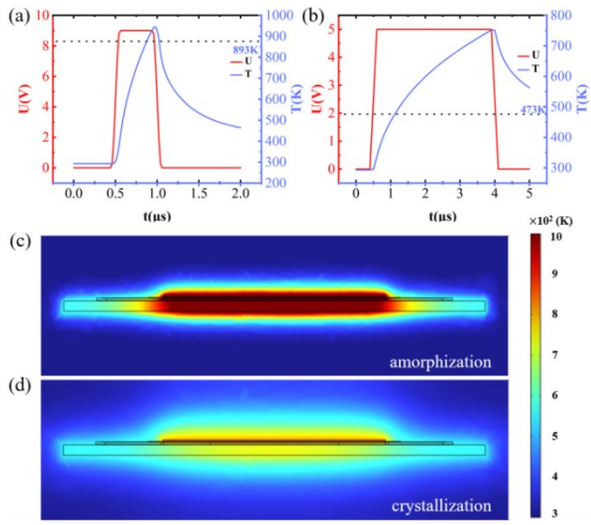


Fig. 6　Thermal simulation of (a) amorphization and (b) crystallization processes. Thermal distribution of the phase-shift arm along longitudinal section at the middle of waveguide for (c) amorphization and (d) crystallization processes
图 6　(a) 非晶化过程的热仿真;(b) 结晶过程的热仿真。在波导中部,相移臂沿纵向截面的热分布:(c) 非晶化过程;(d) 结晶过程

temperature 473 K and the melting point 893 K. A low and long pulse with 5 V amplitude and 3.5 μs width is used, as shown by the red line in Fig. 6(b). Similarly, the whole $Sb_2Se_3$ realizes crystallization, as shown by the blue line in Fig. 6(b) and Fig. 6(d). The corresponding power consumption is about 105.86 nJ. The introduction of the π/2 pre-bias structure reduces the required length of $Sb_2Se_3$, which reduces the power consumption for phase transition of $Sb_2Se_3$. Additionally, the ITO heater we designed fully covers and contacts the $Sb_2Se_3$, enhancing the heating efficiency and further minimizing the energy loss. Table 2 summarizes a comparison for the performance of the 2×2 nonvolatile optical switches in the literature with our work. Our 2×2 MZI nonvolatile optical switch exhibits outstanding characteristics in terms of PCMs length, bandwidth, ER and IL. Moreover, the IL can be further reduced by introducing a coupler structure between the Si waveguide and the Si-$Sb_2Se_3$-ITO waveguide or by designing micro-nano structured $Sb_2Se_3$.

## 3　Conclusions

We demonstrated a broadband high-extinction-ratio 2×2 MZI nonvolatile silicon-based optical switch based on phase change material $Sb_2Se_3$. By introducing a π/2 pre-biased waveguide structure, only 2.71 μm long $Sb_2Se_3$ is needed to tune the switch state, which reduces the absorption loss of crystalline $Sb_2Se_3$ and the power consumption for the phase transition of $Sb_2Se_3$. When $Sb_2Se_3$ in the lower and upper phase-shift arms are at crystalline and amorphous states, respectively, light outputs from the bar port. The IL is 0.84 dB and the ER reaches 28.8 dB at the wavelength of 1550 nm. Inversely, light outputs from the cross port with an IL of 0.84 dB and an ER of 19.8 dB at the wavelength of 1550 nm. At both states, the 3 dB bandwidth is greater than 150 nm. The ER is greater than 20.3 dB and 16.3 dB at bar and cross states in the 3 dB bandwidth, respectively. We used a low and long pulse with 5 V amplitude and 3.5 μs width to achieve the crystallization and a high and short pulse (9 V amplitude, 500 ns width) for amorphization. The corresponding power consumption is 105.86 nJ and 49

**Table 2　Comparison of the reported 2×2 nonvolatile optical switches with our work.**
**表 2　此工作与已报道的 2×2 非易失性光开关的比较**

| | Structure | PCM | PCMs Length | IL(@1550 nm) | BW[1] | ER | Phase transition approach | Power | S/E[2] |
|---|---|---|---|---|---|---|---|---|---|
| Jiang[25] | 3W[3] DC[4] | GSST[5] | 12 μm | Bar: 1.14 dB Cross: 0.38 dB | 100 nm | Bar: >12.3 dB Cross: >10.27 dB | / | / | S |
| Song[26] | MSW[6] | $Sb_2S_3$ | 9.4 μm | Bar: 0.073 dB Cross: 0.055 dB | 35 nm | Bar: >13.6 dB Cross: >15.3 dB | PIN heater | / | S |
| Yang[27] | MZI | $Sb_2S_3$ | 9 μm | Bar: 1.69 dB Cross: 2.93 dB @1543.85 nm | ≈10 nm | Bar: >10 dB Cross: >10 dB | RTA[7] | / | E |
| | | | 3.88 μm | Bar: 0.6 dB Cross: 0.6 dB | ≈40 nm | Bar: >20 dB Cross: >20 dB | / | / | S |
| Yang[28] | MZI | $Sb_2Se_3$ | 18 μm | Bar: 2.5 dB Cross: 2.5 dB | 60 nm | Bar: >20 dB Cross: >20 dB | PIN heater | ≈1 μJ / ≈100 nJ | E |
| Li[29] | MZI/DC | $Sb_2Se_3$ | 1.63 μm | Bar: 0.068 dB Cross: 0.034 dB | 64 nm | Bar: >15 dB Cross: >15 dB | / | / | S |
| Shang[30] | MMI | $Sb_2Se_3$ | ~27 μm | Bar: 1.16 dB Cross: 0.66 dB @1570 nm | 35 nm | Bar: >15 dB Cross: >15 dB | RTA | / | E |
| This work | MZI | $Sb_2Se_3$ | 2.71 μm | Bar: 0.84 dB Cross: 0.84 dB | 150 nm | Bar: >20.3 dB Cross: >16.3 dB | ITO heater | 105.86 nJ / 49 nJ | S |

[1]BW: Bandwidth, [2]S/E: Simulation/Experiment, [3]3W: 3 Waveguide, [4]DC: Directional coupler, [5]GSST: $Ge_2Sb_2Se_4Te_1$, [6]MSW: Multimode slot waveguide, [7]RTA: Rapid thermal annealing.

nJ, respectively. To the best of our knowledge, we have achieved an excellent 2×2 MZI nonvolatile optical switch, which is better than other 2×2 nonvolatile optical switches especially in terms of bandwidth, ER, and IL. Because of the superior characteristics, our optical switch holds considerable potential in the field of optical interconnects and optical computing.

## Acknowledgment

The work is supported by the National Natural Science Foundation of China (No. 62204250) and the Autonomous deployment project of State Key Laboratory of Materials for Integrated Circuits (No. SKLJC-Z2024-A05).

## References

[1] Shastri B J, Tait A N, Ferreira De Lima T, et al. Photonics for artificial intelligence and neuromorphic computing [J]. Nature Photonics, 2021, 15(2): 102-14.
[2] Goi E, Zhang Q M, Chen X, et al. Perspective on photonic memristive neuromorphic computing [J]. Photonix, 2020, 1(1):
[3] Tucker R S, Hinton K. Energy consumption and energy density in optical and electronic signal processing [J]. IEEE Photonics Journal, 2011, 3(5): 821-33.
[4] Tan J Y S, Cheng Z, Feldmann J, et al. Monadic pavlovian associative learning in a backpropagation-free photonic network [J]. Optica, 2022, 9(7): 792-802.
[5] Zhang Y, Chou J B, Li J, et al. Broadband transparent optical phase change materials for high-performance nonvolatile photonics [J]. Nature Communications, 2019, 10(1): 4279.
[6] Orava J, Greer A L, Gholipour B, et al. Characterization of supercooled liquid $Ge_2Sb_2Te_5$ and its crystallization by ultrafast-heating calorimetry [J]. Nature Materials, 2012, 11(4): 279-83.
[7] Shportko K, Kremers S, Woda M, et al. Resonant bonding in crystalline phase-change materials [J]. Nature Materials, 2008, 7(8): 653-8.
[8] Loke D, Lee T H, Wang W J, et al. Breaking the speed limits of phase-change memory [J]. Science, 2012, 336(6088): 1566-9.
[9] Zhang Q, Zhang Y, Li J, et al. Broadband nonvolatile photonic switching based on optical phase change materials: beyond the classical figure-of-merit [J]. Opt Lett, 2018, 43(1): 94-7.
[10] Abdollahramezani S, Hemmatyar O, Taghinejad H, et al. Tunable nanophotonics enabled by chalcogenide phase-change materials [J]. Nanophotonics, 2020, 9(5): 1189-241.
[11] Zhang H, Zhou L, Xu J, et al. Nonvolatile waveguide transmission tuning with electrically-driven ultra-small GST phase-change material [J]. Science Bulletin, 2019, 64(11): 782-9.
[12] Zhang H, Zhou L, Lu L, et al. Miniature multilevel optical memristive switch using phase change material [J]. ACS Photonics, 2019, 6(9): 2205-12.
[13] Xu P, Zheng J, Doylend J K, et al. Low-loss and broadband nonvolatile phase-change directional coupler switches [J]. ACS Photonics, 2019, 6(2): 553-7.
[14] Wu C, Yu H, Li H, et al. Low-loss integrated photonic switch using subwavelength patterned phase change material [J]. ACS Photonics, 2019, 6(1): 87-92.
[15] Li W, Cao X, Song S, et al. Ultracompact high-extinction-ratio nonvolatile on-chip switches based on structured phase change materials [J]. Laser & Photonics Reviews, 2022, 16(6): 2100717.
[16] Ríos C, Du Q Y, Zhang Y F, et al. Ultra-compact nonvolatile phase shifter based on electrically reprogrammable transparent phase change materials [J]. Photonix, 2022, 3(1):
[17] Sun C, Wei M, Tang B, et al. High-performance silicon PIN diode switches in the 2-μm wave band [J]. Opt Lett, 2022, 47(11): 2758-2761.
[18] Li H H. Refractive index of silicon and germanium and its wavelength and temperature derivatives [J]. Journal of Physical and Chemical Reference Data, 1980, 9(3): 561-658.
[19] Malitson I H. Interspecimen comparison of the refractive index of fused silica [J]. J Opt Soc Am, 1965, 55(10): 1205-1209.
[20] Tran M A, Komljenovic T, Hulme J C, et al. A robust method for characterization of optical waveguides and couplers [J]. IEEE Photonics Technology Letters, 2016, 28(14): 1517-20.
[21] Babicheva V E, Kinsey N, Naik G V, et al. Towards CMOS-compatible nanophotonics: ultra-compact modulators using alternative plasmonic materials [J]. Opt Express, 2013, 21(22): 27326-37.
[22] Parra J, Hurtado J, Griol A, et al. Ultra-low loss hybrid ITO/Si thermo-optic phase shifter with optimized power consumption [J]. Opt Express, 2020, 28(7): 9393-404.
[23] Rios C, Stegmaier M, Cheng Z, et al. Controlled switching of phase-change materials by evanescent-field coupling in integrated photonics [Invited] [J]. Opt Mater Express, 2018, 8(9): 2455-70.
[24] Mohammadi-Pouyan S, Afrouzmehr M, Abbott D. Ultra compact bend-less mach-zehnder modulator based on GSST phase change material [J]. Opt Mater Express, 2022, 12(8): 2982-94.
[25] Jiang W. Reconfigurable mode (de) multiplexer via 3-D triple-waveguide directional coupler with optical phase change material [J]. Journal of Lightwave Technology, 2019, 37(3): 1000-7.
[26] Song C, Gao Y, Wang G, et al. Compact nonvolatile 2×2 photonic switch based on two-mode interference [J]. Opt Express, 2022, 30(17): 30430-40.
[27] Yang X, Nisar M S, Yuan W, et al. Phase change material enabled 2 × 2 silicon nonvolatile optical switch [J]. Opt Lett, 2021, 46(17): 4224-7.
[28] Yang X, Lu L, Li Y, et al. Non-volatile optical switch element enabled by low-loss phase change material [J]. Advanced Functional Materials, 2023, 33(42): 2304601.
[29] Li H, Zeng D, Huang Y, et al. Ultra-compact, ultra-low-loss and broadband 2 × 2 nonvolatile optical switch based on $Sb_2Se_3$ phase change material [J]. Opt Express, 2024, 32(20): 35287-97.
[30] Shang K, Niu L, Jin H, et al. Non-volatile 2 × 2 optical switch using multimode interference in an $Sb_2Se_3$-loaded waveguide [J]. Opt Lett, 2024, 49(3): 722-5